Int J Adv Manuf Technol (2014) 74:1637–1648
DOI 10.1007/s00170-014-6119-6

ORIGINAL ARTICLE

A three-dimensional heat conduction inverse procedure to investigate tool–chip thermal interaction in machining process

Vahid Norouzifard · Mohsen Hamedi

Received: 30 December 2013 / Accepted: 27 June 2014 / Published online: 6 July 2014
© Springer-Verlag London 2014

Abstract The present work is set to study the thermal contact phenomena in the tool–chip contact area, which affects the tool life and product quality in the machining process. The objective of this paper is to develop a reliable, efficient, and easy-to-use method for determining important and useful parameters required to study the thermal phenomena in the interface such as the thermal heat flux flowing into the cutting tool and the temperature distribution in the cutting tool. To estimate the heat flux, an inverse procedure is developed based on the sequential function specification (SFS) method. The thermocouples inserted into the specific locations of the cutting tool provide the inverse solver input data during the machining tests performed on AISI 1045 and AISI 304 steels. Future time regularisation method is used to reduce the errors caused by noise in the measured data. Temperature distribution in the tool is computed by performing transient thermal analysis using a 3D finite element model of the cutting tool. The effects of the machining parameters such as cutting speed and feed rate as well as the workpiece material properties on the thermal heat flux and tool temperature in the tool–chip interface are investigated and discussed considering the heat generation and propagation in the secondary deformation zone. The results of the research provide good insight into the effects of the machining parameters, workpiece properties, and tool surface quality on the thermal phenomena in the tool–chip interface.

Keywords Machining · Heat flux · Cutting tool · Tool temperature · Inverse method · ANSYS APDL

V. Norouzifard (✉) · M. Hamedi
School of Mechanical Engineering, College of Engineering, University of Tehran, Tehran, IranP.O. Box 11155/4563
e-mail: v.norouzi.fard@ut.ac.ir

1 Introduction

Machined materials are subject to large plastic deformations during machining process. More than 90 % of the mechanical work applied to the workpiece material transforms to thermal energy [1–4]. Thermal energy spreads in the tool, the work material, and the newly deformed chip. Figure 1 shows the cross-section of the tool, chip, and workpiece near the cutting area. The heat generation zones and schematics of the heat propagation near the tool–chip contact area are also shown in this figure. There are three heat generation zones corresponding to the plastic deformation zones around the tool–chip contact area. Firstly, heat is generated in the primary deformation zone (PDZ) due to shear deformation at the workpiece material. Depending on the cutting velocity, specified fraction of the generated heat in this zone diffuses to the workpiece material and the rest is removed by the chip. Secondly, in the secondary deformation zone (SDZ), the mechanical work applied to overcome friction in the tool–chip interface is converted to heat. The generated heat in SDZ is divided between the tool and the chip. Finally, at the tertiary deformation zone (TDZ), the generated heat due to the friction between the tool flank face and the newly machined surface causes temperature rise in the machined surface and the cutting tool [5].

The mechanical contact phenomena in the tool–chip interface such as normal stress and friction on the tool rake face affects the tool life and product quality in the machining process. Furthermore the tool–chip thermal contact phenomena significantly affect the tool life. Therefore, the tool–chip interface thermal condition has been an interesting issue for experimental and numerical studies of the machining process. Thermal heat flux flowing into the cutting tool and the tool temperature are two important and useful parameters to study thermal phenomena in the interface. The present work is set to study the thermal contact phenomena in the tool–chip contact

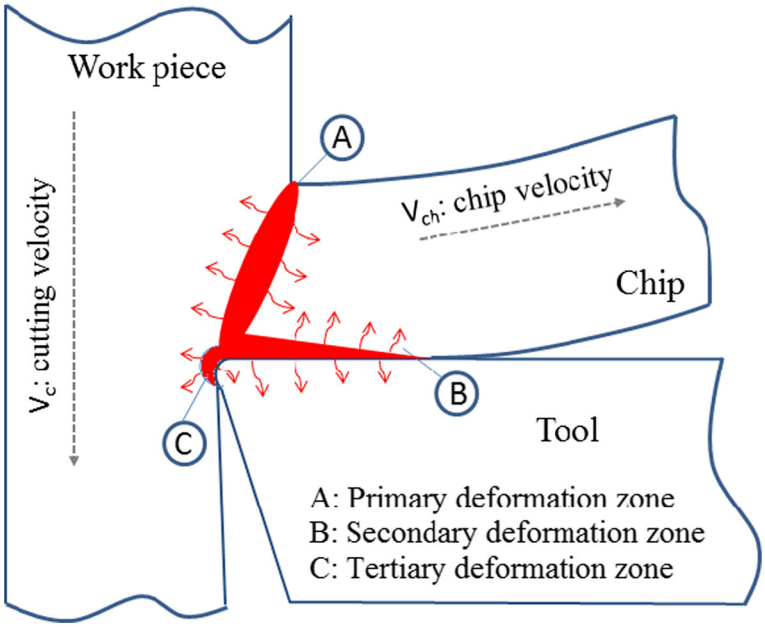

Fig. 1 Schematics of heat generation zones and heat propagation in the machining process

area experimentally. In this paper, an inverse method is developed to determine the thermal heat flux flowing into the cutting tool as well as the tool temperature distribution during machining process.

The most common approach in the literature [6–8] to determine the heat flux flowing into the cutting tool is based on the finite element simulation. Filice et al. [6] developed a 2D finite element (FE) thermo-mechanical model to estimate the heat flux flowing into the tool in orthogonal cutting of AISI 1045 steel. They tuned the FE simulation using temperature data measured by a thermocouple inserted in the cutting tool near the tool–chip contact area. Then, they [6] used the estimated heat flux as boundary condition in a 3D thermal FE model of the cutting tool to calculate temperature distribution in the tool. Although numerical simulation of the cutting process has enjoyed advances during the last decade, this method has a number of limitations in thermal aspects, which are not completely solved yet. The main limitation of this method is the fact that in 2D FE models only small part of a 3D cutting problem is modelled due to restrictions in computers processing power. In addition, in the above-mentioned researches and most of the literature [6, 7, 9–11], thermocouples are always embedded in the holes drilled so close to the tool–chip contact area. Therefore, in the above-mentioned method, the direction of thermocouple is parallel to the heat flux flowing into the tool and high temperature gradients near the tool–chip contact area. Dour et al. [12, 13], and Davies et al. [14] recommended to accommodate thermocouples not only perpendicular to the heat flux but also far from the high temperature gradients. In fact, the hot junction of a thermocouple placed in the high temperature gradient measures the average temperature of the temperature field, whereas, in FE simulation, the average temperature of the thermocouple's top surface is assumed to be the measured temperature by the thermocouple. Grzesik [8] applied the same approach and used tool–chip thermocouple to measure the tool–chip interface average temperature. The tool–chip thermocouple only displays the average temperature between the tool and the chip in the tool–chip contact area without any detailed data about temperature distribution in the tool and the chip.

Inverse methods also have been used to predict temperature and heat flow in the machining process. Yen and Wrigth [15] considered only the cutting tool insert in steady-state condition and estimated heat flux and tool temperature by inverse method. Lin [16] applied least square inverse scheme to determine moving heat source in milling operation from the work surface temperature data. The same approach has been used by Kwon et al. [17] to determine the cutting tool steady-state temperature and heat flux in machining operation on the lathe. Aforementioned inverse models [15–17] applied simplifications either in the problem geometries or thermal solution conditions. Huang et al. [18] utilised an inverse method to estimate the heat flux flowing to the tool during titanium drilling operation. They developed a three-dimensional thermal model of the tool and used steepest decent method to complete inverse procedure. Carvalho et al. [19] developed a three-dimensional model for the tool and holder in turning process. They used the finite difference method and golden section technique followed by a polynomial approximation as direct and inverse thermal solver, respectively. In finite difference method, the tool model is meshed with structured grades. In the complicated geometries, geometrical simplifications are needed to mesh the model using this type of grades. Huang et al. [18] and Carvalho et al. [19] used the temperature data

measured by thermocouples inserted in the cutting tool as input data for inverse solver. Recently, Liang et al. [20] developed a three-dimensional model in which finite deference and conjugate gradient methods are direct and inverse thermal solvers, respectively. To provide input data for inverse solution, Liang et al. [20] measured temperature of specified points on the tool rake face by an infrared (IR) camera. Temperature measurement using IR camera has more difficulties in calibration and installation on the machine tool rather than thermocouples. The aim of the present study is to develop an accurate, reliable, efficient, and easy-to-use inverse procedure to predict the thermal heat flux and temperature distribution on the tool rake face. Furthermore, using a sequential inverse method enables the present model to be suitable for monitoring of the tool thermal condition.

In this paper, thermal heat flux flowing into the cutting tool is determined by inverse method. Inverse thermal solver was programmed in ANSYS parametric design language (APDL) based on sequential function specification (SFS) method [21]. K-type thermocouples accommodated in specified locations of the cutting tool supplied the inverse solver input data. Future time regularisation method [22] was used to reduce the errors arisen from noises in the measured data. A 3D FE model was developed in ANSYS commercial finite element code for direct thermal solution of the cutting tool and the tool holder. Temperature distribution in the cutting tool and average temperature in the tool–chip contact area were estimated by performing transient thermal analysis on the cutting tool. Cutting experiments were conducted on a 2-mm thick tube work material using uncoated carbide cutting tools in the orthogonal cutting condition. In order to investigate the workpiece material thermal properties and machinability effects on the tool thermal condition during machining process, two types of steel with different thermal properties and machinability were considered as workpiece material: AISI 1045 and AISI 304. The effects of cutting parameters such as cutting velocity and feed rate on the heat flux and temperature in the tool–chip interface are also studied as well.

2 Experimental set-up

The machining experiments were performed on a 7-kW lathe machine. Workpieces were 2-mm thick steel tubes with 50 and 60 mm outer diameters made from AISI 1045 steel and AISI 304 stainless steel, respectively. The ISO P30-uncoated carbide inserts with a rake angle of 0° and a relief angle of 6° were used as cutting tool. An appropriate tool holder was designed and manufactured from AISI 1045 steel. In order to avoid the effects of the tool wear on the experiments consistency, a new insert was used for each experiment. Chemical composition and the thermal properties of the cutting tools and work materials [23] are listed in Tables 1 and 2. K-type thermocouples were inserted on the cutting tool in specified situations toward the tool–chip contact area. Figure 2 shows the experimental set-up and a close view of a thermocouple and hole fabricated on the cutting insert to accommodate thermocouple. As mentioned in the previous section, it is recommended in the literature [12–14] to place the thermocouples in positions far from high temperature gradients and perpendicular to thermal flow in the cutting tool. Therefore, before determination of thermocouples arrangement, the direct thermal solution of the tool was done by known heat flux on the tool–chip contact area. According to the temperature distribution of the cutting tool results from thermal solution, appropriate locations of thermocouples were specified. Figure 3 shows the cutting tool CAD model, part of the meshed model near the tool–chip contact area and the thermocouple locations. The tool–chip contact area is also marked in Fig. 3. Thermocouple location and centre point of the tool–chip contact area coordinates are listed in Table 3 according to the Cartesian coordinate system shown in Fig. 3. The origin of the coordinate system is at the right top corner of the tool holder marked with “O” in Fig. 3b. After the thermocouple arrangement was designed, 1.5-mm deep holes with 0.90 mm diameter were made in the determined positions by electrodischarge machine (EDM) super drill to accommodate thermocouples. An appropriate fixture was used to ensure that the thermocouples will be accommodated in the same positions in all cutting tests. Copper nano-powder was used to ensure perfect thermal contact between thermocouples and holes. The temperature data were collected using Omron-Rx 25 data logger, which has 10 channels, and each channel can record temperature data with the sample time of 100 ms. Cutting forces were measured by a Kistler 3D piezoelectric dynamometer during machining experiments. The cutting tool, holder, workpiece, thermocouples, data logger and dynamometer are shown in Fig. 2.

Two series of experiments were designed to study effects of the feed rate and the cutting speed on the thermal behaviour of the work materials during the cutting process. In the first one, feed rate was 0.11 mm/rev and kept constant, and cutting speed was varied from 30 to 125 m/min, while in the other one, cutting speed was kept constant at 89 m/min and feed rate increased from 0.05 to 0.16 mm/rev.

Table 1 Chemical composition of work materials

	Fe	C %	Si %	Mn %	Cr %	Ni %
AISI 1045	Base	0.42	0.25	0.8	0.03	0.02
AISI 304	Base	0.03	0.38	0.92	18.0	8.1

Table 2 Thermal properties of the cutting tool and work materials [23]

	Density (kg/m^3)	Thermal conductivity (W/m °C)	Specific heat capacity (J/kg °C)
Tool (ISO P30 grade)	15,000	43.1	194
AISI 1045	7,800	45	480
AISI 304	7,930	16	480
Air at 300 K	1.205	0.026	1,005

In order to study the thermal interaction between the cutting tool and the chip as well as modelling the heat flux entrance area on the cutting tool rake face, accurate measurement of the tool–chip contact area is essential. Using an image processing software [24], chemical analysis of the cutting tool rake surface [25] and observation of the contact area by optical microscope [26] or scanning electron microscope (SEM) [27] have been used in the available literature to measure the contact area. In all cases, the contact area was measured after the cutting operation. Here, an optical microscope in addition with an image processing software was used to measure the tool–chip contact area. Figure 4 shows an optical microscopy image taken with 50× magnification.

3 Inverse solution

The transient three-dimensional heat diffusion equation can be written as

$$\frac{\partial^2 T}{\partial x^2}+\frac{\partial^2 T}{\partial y^2}+\frac{\partial^2 T}{\partial z^2}=\frac{\rho C_p}{k}\frac{\partial T}{\partial t} \tag{1a}$$

where T, C_p, k and ρ are temperature, specific heat capacity, thermal conductivity and density, respectively. The initial condition is:

$$T(x,y,z,t)=T_0 \tag{1b}$$

where T_0 is the initial temperature. The boundary condition of the tool–chip contact area is:

$$-k\frac{\partial T}{\partial \eta}=q(t) \tag{1c}$$

where η is the outward normal vector of the subject surface, and q is the time dependent heat flux flowing into the tool. The boundary condition of the tool areas exposed to the environment is:

$$-k\frac{\partial T}{\partial \eta}=h(T-T_\infty) \tag{1d}$$

where h and T_∞ are the convective heat transfer coefficient and ambient temperature. The boundary condition of the contact areas between the tool and tool holder is:

$$-k\frac{\partial T}{\partial \eta}=h_c(T-T_\infty) \tag{1e}$$

where h_c is the thermal contact conductance (TCC).

In a direct thermal problem, all boundary condition and material properties are known. If a part of the direct problem description such as a boundary condition or a material property is missing and is to be found, the problem is known as the inverse problem. Instead of the missing part, supplementary data are available from experimental tests. In the present inverse problem, the heat flux flowing into the tool was the unknown part. The heat flux was estimated using the thermocouple temperature data measured from specified locations on the tool.

3.1 Inverse theoretical fundamentals

Using superposition principles and Duhamel's superposition integral, the following solution [21] can be written for Eqs. (1a, 1b, 1c, 1d and 1e):

$$T(x,y,z,t)=T_0(x,y,z,t)-\int_0^t q(\lambda)\frac{\partial \varphi(x,y,z,t-\lambda)}{\partial \lambda}\mathrm{d}\lambda \tag{2}$$

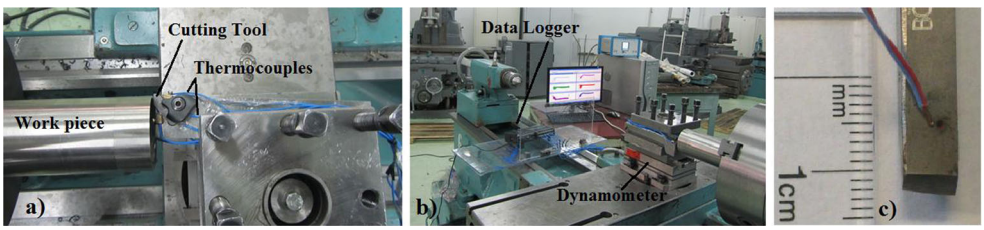

Fig. 2 **a**, **b** Experimental set-up and **c** close view of cutting tool, thermocouple location and a thermocouple

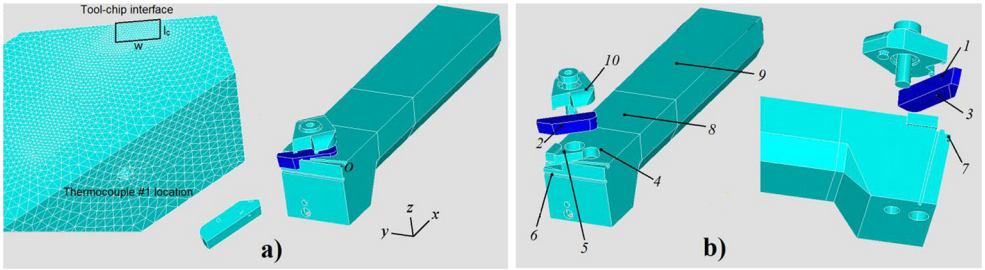

Fig. 3 Cutting tool and tool holder CAD models: **a** 3D CAD model, close view of the meshed cutting tool and the tool–chip interface and **b** thermocouples location

where $\varphi(x,y,z,t)$ is the unit impulse response and is the solution of Eqs. (1a, 1b, 1c, 1d and 1e) with a constant input heat flux in the tool–chip interface ($q(t)=1$ in Eq. (1c)). Considering discrete form of Eq. (2) with fixed time intervals, temperature of the point (x_i,y_i,z_i) at time t_M can be calculated by:

$$T(x_i,y_i,z_i,t_M) = T_0 + \sum_{n=1}^{M} q_n \Delta\varphi_{(M-n)} \tag{3}$$

where

$$\Delta\varphi_{(M-n)} = \varphi(x_i,y_i,z_i,t_{M-n+1}) - \varphi(x_i,y_i,z_i,t_{M-n}) \tag{4}$$

Assuming piecewise-constant heat flux components in equal time intervals instead of the time-dependent heat flux function appeared in Eq. (1c) and based on Eq. (3), if all components of the heat flux are determined for $t=\Delta t, 2\Delta t, 3\Delta t, \ldots, (M-1)\Delta t$, then the next heat flux component, $\widehat{q}_M$, for $t=M\Delta t=t_M$ will be computed as

$$\widehat{q}_M = \frac{Y_{iM} - \widehat{T}(x_i,y_i,z_i,t_{M-1})}{\Delta\varphi_0} \tag{5}$$

where $\widehat{T}(x_i,y_i,z_i,t_{M-1})$ is the temperature at the measurement location (x_i,y_i,z_i) and can be estimated by Eq. (3) based on all calculated heat flux components before $\widehat{q}_M$. Y_{iM} is the measured temperature at time t_M.

Inverse problems are called ill-posed problems and need the regularisation methods to be a well-posed problem [21]. The common way to add regularisation to the inverse problems is minimising of the error between the computed results and measured data with respect to the unknown heat flux. Traditional error minimisation approach is minimising the least square function S, as:

$$S_m = \sum_{i=1}^{r} \left(Y_{m+i-1} - T_{m+i-1}\right)^2 \tag{6}$$

where T, Y are the calculated and measured temperatures, respectively. In the present work, the SFS method [21] together with future time regularisation method [22] was used. Based on these methods, the heat flux component $\widehat{q}_M$ at time t_M can be estimated by.

$$\widehat{q}_M = \frac{\sum_{i=1}^{r} \varphi_i \left(Y_{M+i-1} - \widehat{T}_{M+i-1}\right)}{\sum_{i=1}^{r} \varphi_i^2} \tag{7}$$

where r is the regularisation parameter. It means that the inverse results regularised using measured temperature data after sequence M where the number of the measured data is equal to r. An inverse procedure needs an optimum value of r to estimate the problem unknown with minimum error. In the present study, to determine optimum regularisation parameter, the following procedure was developed: first, transient heat transfer problem of the tool with known heat flux on the tool–chip contact area was solved by direct solver and the temperature history of the thermocouple locations were calculated numerically. In the second step, artificially generated noises were added to the calculated temperature data. The heat flux flowing into the tool was reconstructed by the inverse solver using artificially generated input data. Finally, the root mean squares of the errors were calculated for various regularisation parameters by:

$$E_{\text{rms}} = \sqrt{\frac{\sum_1^N \left((q_{\text{exact}})_i - (q_{\text{calculated}})_i\right)^2}{N}} \tag{8}$$

Table 3 Thermocouples situation coordinates

Thermocouple no.	X (mm)	Y (mm)	Z (mm)
T1	4.76	30.6	−0.78
T2	0.82	22.3	−0.15
T3	5.97	24.3	−5.00
T4	1.5	29.5	−7.00
T5	1.2	34.00	−6.1
T6	11.4	23.00	0
T7	16.5	8.7	0
T8	48.5	14.5	0
T9	95.0	16.00	0
T10	15.2	15.2	8.85
Tool–chip contact area centre point	0.27–0.83	30.0	1.0

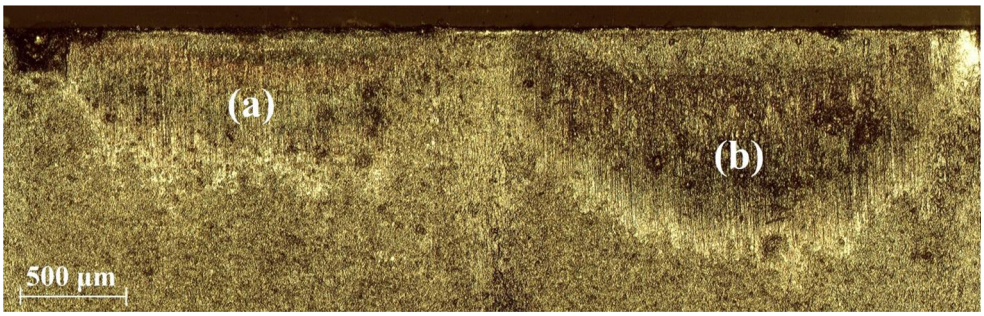

Fig. 4 Optical microscopy image of the tool–chip contact area of AISI 1045 machining at **a** cutting speed of 90 m/min and feed rate 0.05 mm/rev and **b** cutting speed of 125 m/min and feed rate 0.11 mm/rev

where i and N are time index and total number of data, respectively.

3.2 FEM model

From Eq. (7), the unit impulse response, $\varphi(x,y,z,t)$, in thermocouples locations is required to calculate the heat flux. To calculate unit impulse response, Eqs. (1a, 1b, 1c, 1d and 1e) should be solved assuming unit heat flux, $q(t)=1$, for the tool–chip interface boundary condition. Here, transient thermal analysis was performed using ANSYS commercial finite element code to solve these equations. A 3D model was developed for the cutting tool and holder. The model was meshed with ANSYS thermal analysis elements. Figure 3 shows 3D CAD geometry and a close view of meshed cutting tool. This figure also shows the tool–chip contact area over which the thermal heat flux was applied. The following boundary conditions were assumed for the model:

1. For all areas of the cutting insert which were exposed to the air, heat loss due to convection (h=20 W/m^2 °C and $T_{ambient}$=25 °C) is considered.
2. Thermal contact was assumed for all interior areas of the cutting tool and holder, which are in contact.
3. A uniform heat flux was applied on the tool surface in tool–chip contact area.

Another important factor, affecting accuracy of the thermal modelling and inverse solution, is the TCC, h_c, between the cutting tool and the tool holder. TCC between two solid bodies in contact together depends on several factors such as surface roughness and thermal properties of the bodies, average contact temperature and normal pressure between the bodies. Carvalho et al.[19] considered an air gap with 10-m thickness between contacting surfaces with an air property at 300 K to simulate thermal contact. In the present work, according to the dimensional differences between the cutting tool and the cavity manufactured on the holder to accommodate it, 20-μm air gap was assumed between the cutting tool side surfaces (S1, S2, and S3 in Fig. 5) and the holder. The cutting tool bottom was divided into two surfaces (B1 and B2 in Fig. 5). The TCC of the surface marked as B2 in Fig. 5 was simulated by 10-μm air gap due to the surface roughness of the contacting surfaces. The air thermal properties are listed in Table 2. Several thermocouples (numbers 4, 5, 6 and 7 listed in Table 3) were accommodated in tool holder near the contact surfaces to monitor the temperature of the holder. The surface named B1 in Fig. 5 is exactly under the cutting area and cutting force applied on the tool rake face can cause high normal pressure between the cutting tool and this surface. Therefore, the TCC in this area can be higher than the rest of the contact areas. To determine the TCC of the surface B1, the temperature data measured by thermocouples 6 and 7 were used. Comparing the temperature measured by these thermocouples with the FEM results through an inverse trial and error procedure, value of 18,000 (W/m^2 °C) was estimated for the TCC between the surface B1 and the cutting tool in the present study. Thermal contacts were simulated using 2D contact elements in finite element model.

4 Results and discussion

As mentioned in Section 3.1, artificial temperature data were used to find optimum value of the regularisation parameter, r. The artificial data were generated solving direct thermal problem by a known time-depended heat flux. Then, the heat flux was reconstructed by inverse solver using different values of r. Figure 6 shows the preliminary heat flux and reconstructed heat fluxes using different regularisation parameters. Figure 7 presents variation of the error, E_{rms} versus the regularisation factor, r. As seen in Fig. 6, increasing the regularisation factor decreases the results fluctuation. Using high regularisation factor also reduces the inverse solver's capability to predict the abrupt changes in heat flux. According to Fig. 7, the root mean square of the errors generated during inverse procedure, E_{rms} has a minimum value in r=20. This value was considered as the regularisation factor in the present study. It means that the heat flux on the tool–chip interface can be estimated with 2-s delay time.

Tables 4 and 5 list input cutting parameters corresponding to the experimental tests performed on AISI

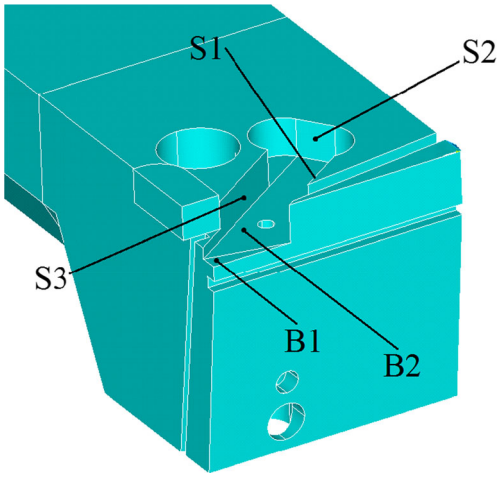

Fig. 5 Surfaces of the tool holder, which are in thermal contact with the cutting tool

1045 and AISI 304, respectively. Some important machining output parameters such as friction forces, chip compression factor and tool–chip contact length are also reported in Tables 4 and 5. In order to examine the repeatability of the experimental results, each experiment was repeated three times. It is necessary to mention that the repetitions were not performed consecutively. Also between two consecutive experiments, an appropriate delay time was applied to ensure that tool and workpiece temperature fields become uniform and steady state. Figure 8a and b shows the estimated heat flux at the tool–chip interface during machining AISI 1045 and AISI 304 under cutting conditions of tests 1 and 2 from Table 4 and test 7 from Table 5, respectively. Some dispersion, <8 %, exists between the estimated heat flux in different repetitions maybe because of uncertainty in thermal properties of the cutting tool, errors in measurements, variation in ambient condition

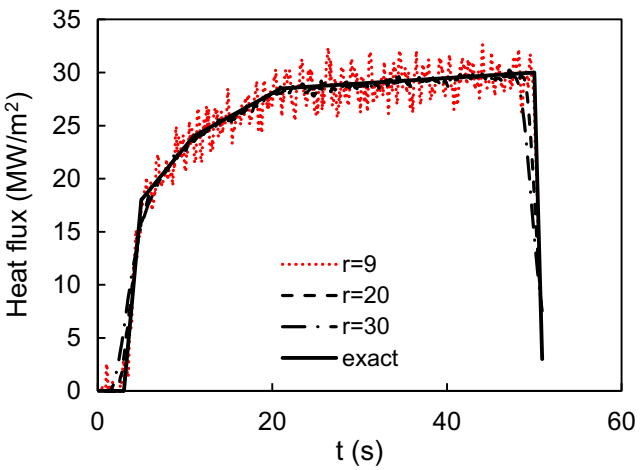

Fig. 6 Estimated heat flux using various regularisation factor, *r*, values

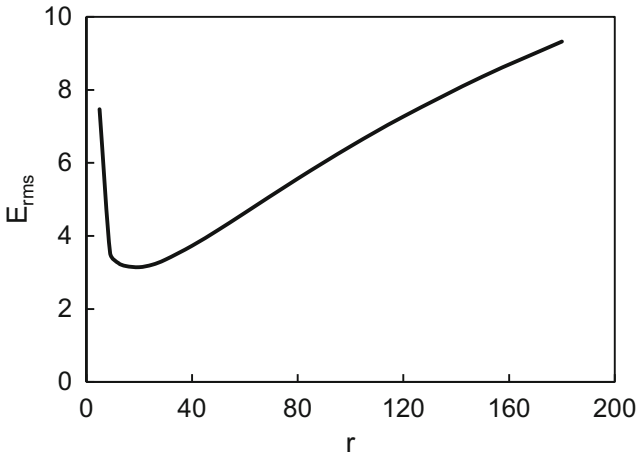

Fig. 7 The root mean square of errors versus regularisation factor *r*

such as the tool holder, machine tool and surrounding temperature, etc.

As seen in Fig. 8, the heat flux flowing into the cutting tool reaches almost steady-state condition 30 s after machining operation start time. Figure 9 shows the average steady-state heat flux versus cutting speed and feed rate. The majority of the heat flux flowing into the cutting tool is generated in the SDZ (see Fig. 1) due to the shear plastic deformation of the chip. According to the literature [1–4], almost all of the mechanical work applied to deform the chip material in the SDZ converts to the heat. Thus, the generated heat in the SDZ can be estimated by:

$$q_f = \frac{F_f V_{ch}}{A_c} = \frac{F_f V_c}{A_c \lambda_{ch}} \tag{9}$$

where F_f, V_{ch}, A_c, V_c are friction force in the tool–chip interface, chip velocity, the tool–chip contact area and cutting velocity, respectively. λ_{ch} is the chip compression factor and can be calculated by dividing the chip thickness over the uncut chip thickness. The chip can be considered as a moving heat source for the tool.

Table 4 Experimental results for AISI 1045 steel material

Test no.	V_c (m/min)	f (mm/rev)	l_c (mm)	λ_{ch}	F_f (N)
1	31.4	0.11	0.99	3.79	450
2	44.5	0.11	0.89	4.3	434
3	63	0.11	0.93	4.2	421
4	89.2	0.05	0.53	4.8	237
5	89.2	0.08	0.68	4.21	295
6	89.2	0.11	0.96	3.85	374
7	89.2	0.14	1.13	3.26	419
8	89.2	0.16	1.11	3.12	442
9	125.7	0.11	0.96	3.67	340

Table 5 Experimental results for AISI 304 steel material

Test no.	V_c (m/min)	f (mm/rev)	l_c (mm)	λ_{ch}	F_f (N)
1	32	0.11	1.59	5.32	540
2	44.5	0.11	1.45	5.25	511
3	63	0.11	1.36	5.31	431
4	89	0.05	1.08	6.8	321
5	89	0.08	1.35	5.33	361
6	89	0.11	1.46	6.18	454
7	89	0.14	1.53	4.01	413
8	89	0.16	1.65	3.27	529
9	126	0.11	1.47	4.82	457

Therefore, Peclet number is a useful parameter to achieve better understanding about heat propagation between the tool and the chip in the tool–chip interface. The Peclet number [28] is calculated as following:

$$\mathrm{Pe}_{ch} = \frac{V_{ch} l_c}{\alpha_T} \tag{10}$$

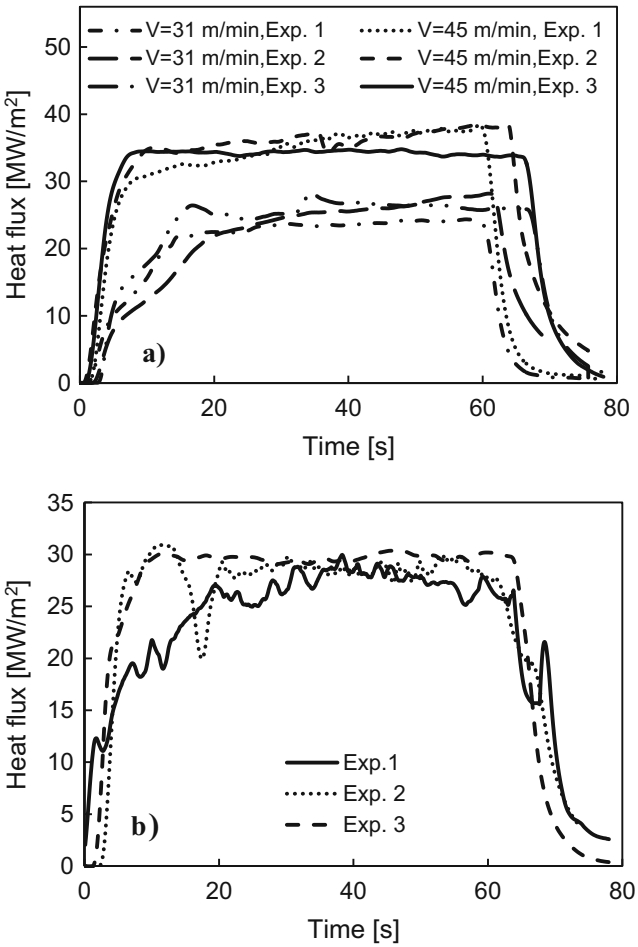

Fig. 8 Comparing calculated heat flux at the tool–chip interface for three repetitions: **a** AISI 1045 workpiece (feed rate=0.11 mm/rev) and **b** AISI 304 (feed rate=0.08 mm/rev and cutting speed=89 m/min)

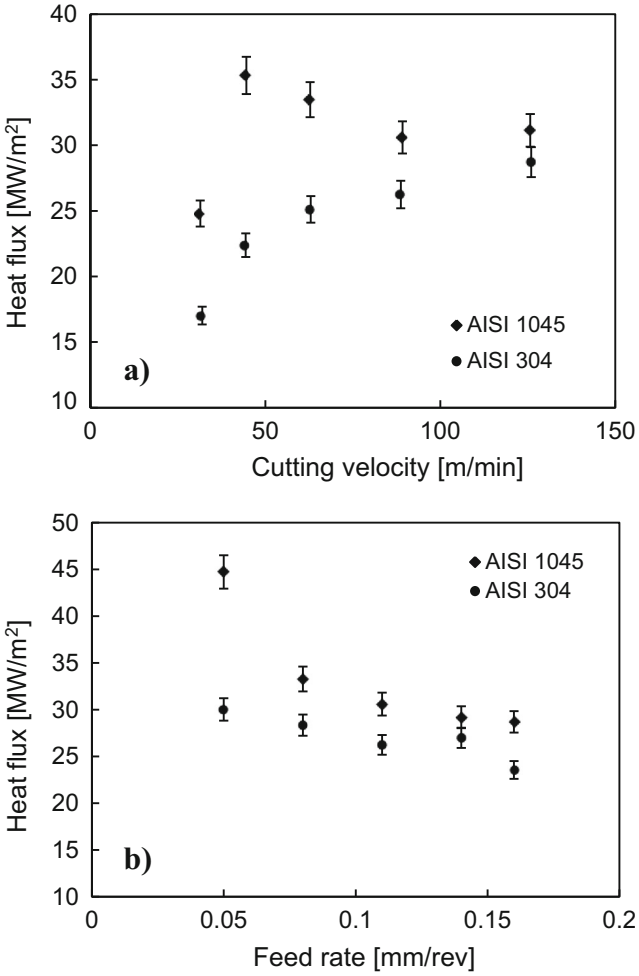

Fig. 9 Thermal heat flux at the tool chip interface versus **a** cutting speed (f=0.11 mm/rev) and **b** feed rate (V_c=89 m/min)

where l_c and α_T are the tool–chip contact length and thermal diffusivity of the tool material. A low Peclet number allows more heat propagation around the heat generation area. Therefore, in the low cutting speeds, high percentage of the generated heat in SDZ flows into the tool (Eq. 10), but the heat generation is still low (Eq. 9). As seen in Fig. 9a, for AISI 1045 machining, the heat flux flowing into the tool rake face increases when cutting speed increases from 31 up to 45 m/min due to the heat generation growth. On the other hand, in the cutting speeds beyond 45 m/min, the heat flux decreases because of Peclet number increasing. For both of the work materials, the heat flux flowing into the cutting tool decreases when the feed rate increases, as shown in Fig. 9b. The more feed rate causes the more chip thickness and diffused heat into the chip material.

The heat partition factor is defined as the ratio of the heat flux flowing into the tool to the total generated heat in the SDZ. Variation of the generated heat flux in the SDZ and heat partition factor are presented versus cutting speed and feed rate in Fig. 10. According to this figure, the heat partition

factor of the AISI 304 is always higher than AISI 1045. In other words, the fraction of the generated heat, which is propagated at the chip for the AISI 304 work material, is less than that in the AISI 1045 steel because of low thermal conductivity and thermal diffusivity of AISI 304. In addition, the heat generation rate at SDZ in the AISI 304 material is less than that in AISI 1045, as shown in Fig. 10. The generated heat is localised in the deformation zone due to the low thermal diffusivity and conductivity of AISI 304. Temperature rise causes thermal softening in the localised deformation zone. Therefore, plastic deformation and heat generation concentrated in a narrow zone.

As mentioned above, to calculate the temperature distribution in the tool, the estimated heat flux by the inverse method was applied on the tool–chip contact area (see Fig. 3a). Then, a transient thermal analysis was performed to calculate temperature fields in the cutting tool. Figure 11 shows the estimated temperature distribution in the cutting tool and the tool holder in the 60th second of machining time of AISI 1045 material under cutting velocity of 89.2 m/min and feed rate of 0.11 mm/rev. As expected, the tool–chip contact area has the maximum temperature in the cutting tool. The part of the tool holder exactly under the tool–chip interface reaches maximum

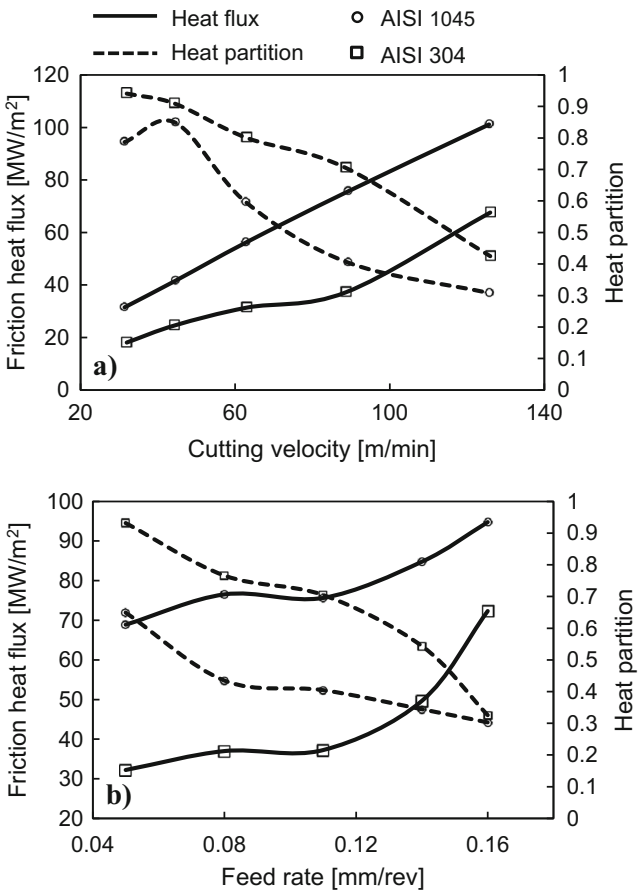

Fig. 10 Friction heat and the heat partition factor at tool–chip interface versus **a** cutting speed (f=0.11 mm/rev) and **b** feed rate (V_c=89 m/min)

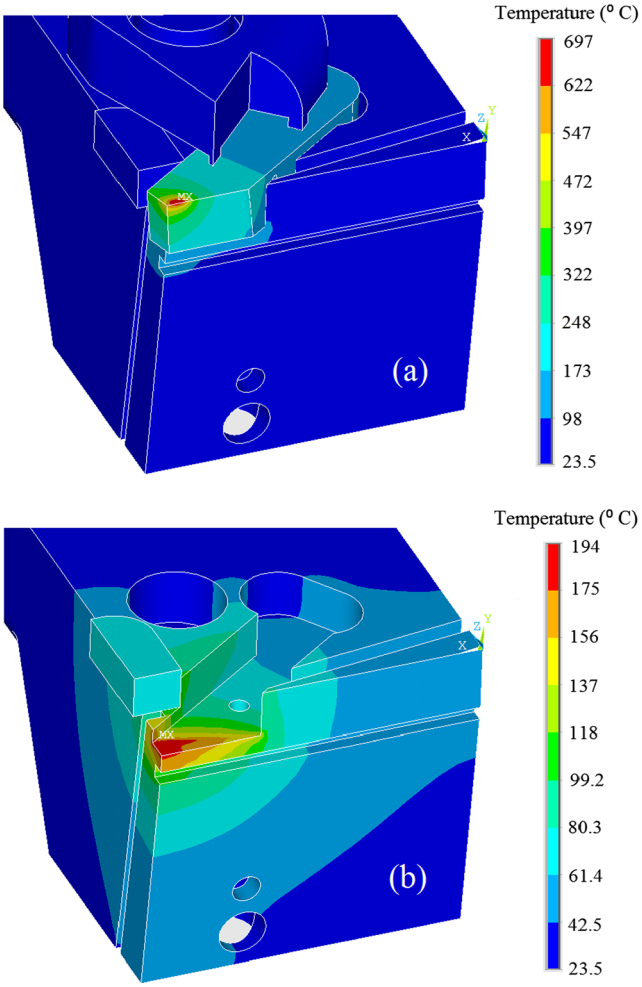

Fig. 11 Temperature distribution in **a** the cutting tool and **b** the tool holder at 60th second of machining of AISI 1045 material under cutting velocity of 89 m/min and feed rate of 0.11 mm/rev

temperature because of high TCC between the tool and the holder in this area.

Temperature history sensed by thermocouples and estimated by FEM during machining of AISI 1045 under cutting condition of test 2 from Table 4 is shown in Fig. 12a and b, respectively. Comparing Fig. 12a and b shows a good agreement between the measured and corresponding estimated temperature history at the thermocouples positions. Difference between the measured (Fig. 12a) and calculated (Fig. 12b) temperature history of the thermocouples locations is also presented in Fig. 12c. According to this figure, errors increase in the machining starting time and the end of machining. The main source of these errors is regularisation used in the inverse procedure. Although regularisation methods reduce the errors arisen from the existing noises in the input data, they add bias errors on the results. These methods deform the shape of the estimated heat flux versus time diagram especially at the regions that the

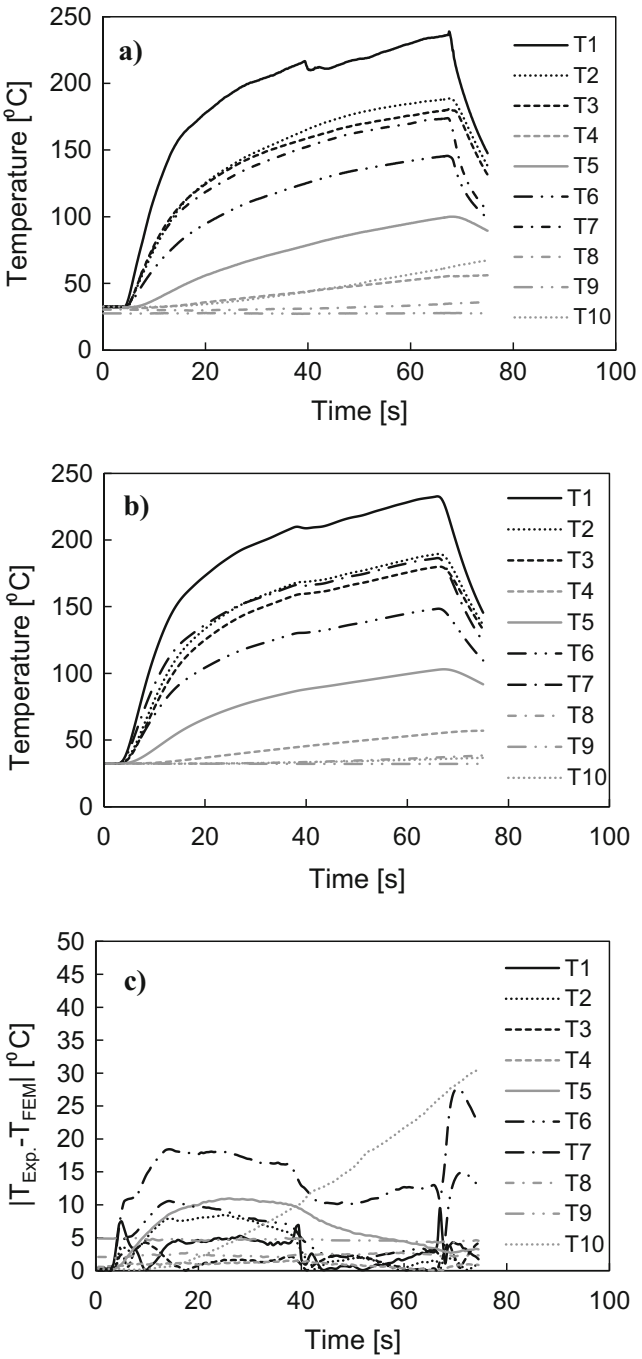

Fig. 12 **a** Thermocouples measured, **b** numerically calculated and **c** difference between measured and numerically calculated temperature history during machining of AISI 1045 steel at cutting velocity of 44.5 m/min and feed rate of 0.11 mm/rev

heat flux changes sharply (the start and the end of machining). Figure 12c also shows considerable unexpected errors between numerically estimated results and the measured data by thermocouple T10. As shown in Fig. 3b, thermocouple T10 is accommodated in the cutting tool clamp. Contact of the hot chip with the tool clamp during the machining tests provides an extra heat source for this part. This heat source has not serious effects on the cutting tool temperature distribution. It was neglected in FE modelling of the tool.

Table 6 lists the estimated and measured maximum temperature by thermocouple T1 for the machining tests and the relative difference between the estimated and measured values. Maximum difference between the measured and regenerated temperature in thermocouple T1 location is ±5 %. Uncertainties in the final tool temperature results arise from the uncertainty sources such as the thermocouples position, the thermocouples measuring accuracy, the tool material thermal properties, measurement of the tool–chip contact area and numerical calculation errors.

The average temperature of the nodes located in the tool–chip contact area was considered as the average tool temperature in the tool–chip interface. The average tool temperature versus the cutting velocity and feed rate diagrams are presented in Fig. 13a and b, respectively. The tool–chip average temperature measured by Grzesik [29] using the tool–chip thermocouple in machining of the AISI 304 steel under cutting condition close to the present work are also presented in Fig. 13. In Fig. 13b, the tool temperature decreases considerably when the feed rate increases from 0.14 to 0.16 rev/mm, whereas the tool–chip thermocouple results measured by Grzesik [29] show slight increasing slope versus feed rate. Increasing feed rate results in the tool–chip length and the Peclet number increase. Thus, in the higher feed rates, heat concentration in the heat generation zone (SDZ) increases due to the Peclet number increase. In addition, tool surface quality can affect the heat transfer phenomena in the tool–chip interface. Even in the smooth surfaces, asperities exist. Therefore, contact is made only at discrete locations, rather than over the entire area. As the surface roughness increases, the number of contact spots and real contact area decreases

Table 6 Comparison between maximum measured temperature by T1 and direct thermal solution results

	AISI 1045			AISI 304		
Test no.	T1	FEM	Error %	T1	FEM	Error %
1	185	195	5.4	202	203	0.5
2	235	231	−1.7	239	236	−1.3
3	216	222	2.8	223	224	0.4
4	174	183	5.2	217	219	0.9
5	188	197	4.8	225	228	1.3
6	194	199	2.6	235	238	1.27
7	188	196	4.3	264	252	−4.5
8	217	205	−5.5	305	294	−3.6
9	205	212	3.4	271	257	−5.1

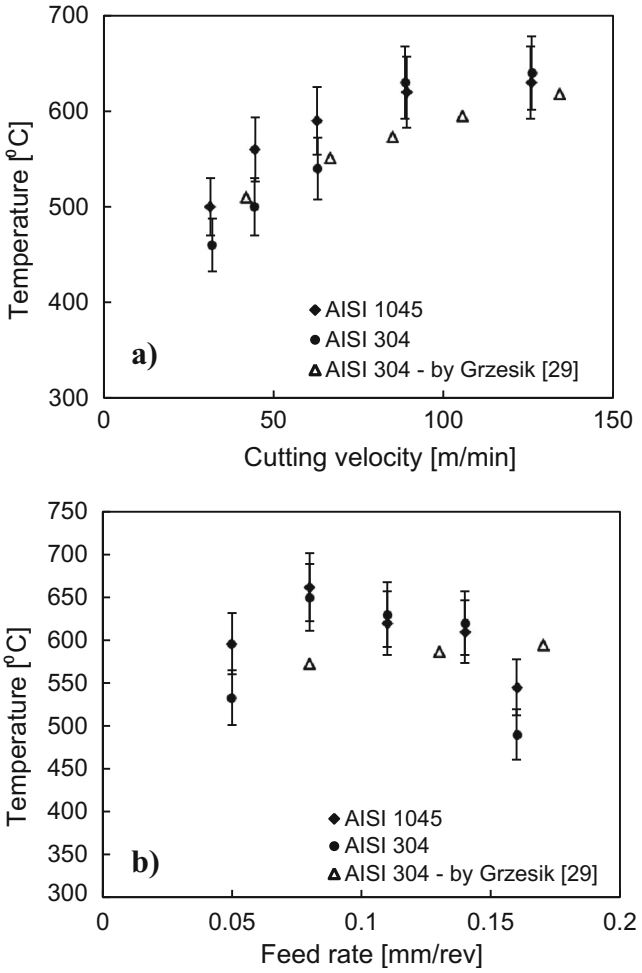

Fig. 13 Average temperature at the tool–chip interface **a** versus cutting speed (f=0.11 mm/rev for present study and f=0.17 mm/rev for Grzesik [29]) and **b** versus feed rate (V_c=89 m/min for present study and V_c= 107 m/min for Grzesik [29])

[30]. Thus, the heat encounters with more thermal resistance to pass the tool–chip interface through the tool. To investigate tool roughness effects on the tool–chip thermal interaction, surface roughness of the cutting tool in the tool–chip contact area was measured by Mitutoyo SJ 400 profilometer. These measurements show that for all tests except the tests performed on AISI 1045 and AISI 304 workpiece materials in the feed rates of 0.14 and 0.16 mm/rev, the average surface roughness, R_a, of the tool–chip contact area has not changed significantly comparing to the initial surface roughness of the cutting tool, which is about 0.7 μm. The average surface roughness of the cutting tools that cut these materials in the feed rates of 0.14 and 0.16 mm/rev are about 0.85 and 1.1 for AISI 1045 and 0.8 and 1.0 μm for AISI 304 machining tests, respectively. Increasing the tool surface roughness in the this area due to tool wear can be another reason of temperature drop in the feed rates higher than 0.14 mm/rev.

5 Conclusions

An inverse solver based on the SFS method was developed in this research. ANSYS finite element code was used as a direct solver to calculate sensitivity coefficients needed for inverse procedure and the tool temperature distribution as well. An experimental set-up was built to provide an input data for the inverse solver. Before beginning the tests, developed inverse program was examined and regulated by artificial input data. In order to study the repeatability of the procedure, each experiment was repeated three times. Comparing the results of the repetitions showed maximum 8 % dispersion between them. In order to investigate effects of the workpiece material properties on the results, two steel materials with different thermal properties were tested, being AISI 1045 and AISI 304.

Satisfactory agreement between the estimated and measured temperature fields at the tool and the holder validates the developed inverse procedure. It also ascertains the procedure capability and reliability to predict temperature distribution as well as the heat flux in the tool–chip interface. SFS method used in the present inverse procedure allows estimating the heat flux on the tool rake face with a small delay time and enhances the capability of the developed methodology for real-time monitoring purposes. The established methodology can be used for better understanding of the tool–chip contact phenomena. The results of the research also provide good insight to effect of machining parameters and some factors such as workpiece thermal properties and tool rake surface quality on the thermal phenomena in the tool–chip interface.

Acknowledgments The authors would like to acknowledge the financial support of the University of Tehran for this research under grant number 8151299/1/04. The authors also would like to give thanks to Navid Khani and Mir Masoud Seyyed Fakhrabadi for their kind assistance in the experiments.

References

1. Iqbal SA, Mativenga PT, Sheikh MA (2007) Characterization of machining of AISI 1045 steel over a wide range of cutting speeds. Part 2: evaluation of flow stress models and interface friction distribution schemes. Proc Inst Mech Eng Part B J Eng Manuf 221:917–926. doi:10.1243/09544054JEM797
2. Molinari A, Cheriguene R, Miguelez H (2012) Contact variables and thermal effects at the tool–chip interface in orthogonal cutting. Int J Solids Struct 49:3774–3796. doi:10.1016/j.ijsolstr.2012.08.013
3. Pawade RS, Sonawane HA, Joshi SS (2009) An analytical model to predict specific shear energy in high-speed turning of Inconel 718. Int J Mach Tools Manuf 49:979–990. doi:10.1016/j.ijmachtools.2009.06.007
4. Ee K, Dillonjr O, Jawahir I (2005) Finite element modeling of residual stresses in machining induced by cutting using a tool with finite edge radius. Int J Mech Sci 47:1611–1628. doi:10.1016/j.ijmecsci.2005.06.001

5. Jam J, Norouzi Fard V (2011) A novel method to determine tool–chip thermal contact conductance in machining. IJEST 3:8491–8501
6. Filice L, Umbrello D, Beccari S, Micari F (2006) On the FE codes capability for tool temperature calculation in machining processes. J Mater Process Technol 174:286–292. doi:10.1016/j.jmatprotec.2006.01.012
7. Filice L, Micari F, Rizzuti S, Umbrello D (2007) A critical analysis on the friction modelling in orthogonal machining. Int J Mach Tools Manuf 47:709–714. doi:10.1016/j.ijmachtools.2006.05.007
8. Grzesik W (2006) Determination of temperature distribution in the cutting zone using hybrid analytical-FEM technique. Int J Mach Tools Manuf 46:651–658. doi:10.1016/j.ijmachtools.2005.07.009
9. Umbrello D, Filice L, Rizzuti S, Micari F (2007) On the evaluation of the global heat transfer coefficient in cutting. Int J Mach Tools Manuf 47:1738–1743. doi:10.1016/j.ijmachtools.2006.12.002
10. Ay H, Yang WJ (1998) Heat transfer and life of metal cutting tools in turning. Int J Heat Mass Transf 41:613–623
11. Ren X, Yang QX, James RD, Wang L (2004) Cutting temperatures in hard turning chromium hardfacings with PCBN tooling. J Mater Process Technol 147:38–44. doi:10.1016/j.jmatprotec.2003.10.013
12. Dour G, Dargusch M, Davidson C (2006) Recommendations and guidelines for the performance of accurate heat transfer measurements in rapid forming processes. Int J Heat Mass Transf 49:1773–1789. doi:10.1016/j.ijheatmasstransfer.2005.10.045
13. Dour G, Dargusch M, Davidson C, Nef A (2005) Development of a non-intrusive heat transfer coefficient gauge and its application to high pressure die casting: effect of the process parameters. J Mater Process Technol 169:223–233. doi:10.1016/j.jmatprotec.2005.03.026
14. Davies M, Ueda T, M'saoubi R et al (2007) On the measurement of temperature in material removal processes. CIRP Ann Technol 56:581–604. doi:10.1016/j.cirp.2007.10.009
15. Yen D, Wright P (1986) A remote temperature sensing technique for estimating the cutting interface temperature distribution. J Eng Ind (Trans ASME) 108:1986
16. Lin J (1995) Inverse estimation of the tool–work interface temperature in end milling. Int J Mach Tools Manuf 35:751–760
17. Kwon P, Schiemann T, Kountanya R (2001) An inverse estimation scheme to measure steady-state tool–chip interface temperatures using an infrared camera. Int J Mach Tools Manuf 41:1015–1030. doi:10.1016/S0890-6955(00)00113-9
18. Huang C-H, Jan L-C, Li R, Shih AJ (2007) A three-dimensional inverse problem in estimating the applied heat flux of a titanium drilling—theoretical and experimental studies. Int J Heat Mass Transf 50:3265–3277. doi:10.1016/j.ijheatmasstransfer.2007.01.031
19. Carvalho SR, Silva SLE (2006) Temperature determination at the chip–tool interface using an inverse thermal model considering the tool and tool holder. J Mater 179:97–104. doi:10.1016/j.jmatprotec.2006.03.086
20. Liang L, Xu H, Ke Z (2013) An improved three-dimensional inverse heat conduction procedure to determine the tool–chip interface temperature in dry turning. Int J Therm Sci 64:152–161. doi:10.1016/j.ijthermalsci.2012.08.012
21. Woodbury K (2003) Inverse engineering handbook. Press, CRC
22. Beck JV, Blackwell BF, St C (1985) Inverse heat conduction Ill-posed problems. Wiley Interscience, New York
23. Grzesik W, Nieslony P (2004) Prediction of friction and heat flow in machining incorporating thermophysical properties of the coating–chip interface. Wear 256:108–117. doi:10.1016/S0043-1648(03)00390-9
24. Grzesik W (2000) The influence of thin hard coatings on frictional behaviour in the orthogonal cutting process. Tribol Int 33:131–140. doi:10.1016/S0301-679X(00)00072-4
25. Courbon C, Mabrouki T, Rech J et al (2012) On the existence of a thermal contact resistance at the tool–chip interface in dry cutting of AISI 1045 : formation mechanisms and influence on the cutting process. Appl Therm Eng. doi:10.1016/j.applthermaleng.2012.06.047
26. Korkut I, Donertas MA (2007) The influence of feed rate and cutting speed on the cutting forces, surface roughness and tool–chip contact length during face milling. Mater Des 28:308–312. doi:10.1016/j.matdes.2005.06.002
27. Kilic DS, Raman S (2007) Observations of the tool–chip boundary conditions in turning of aluminum alloys. Wear 262:889–904. doi:10.1016/j.wear.2006.08.019
28. Grzesik W, Nieslony P (2003) A computational approach to evaluate temperature and heat partition in machining with multilayer coated tools. Int J Mach Tools Manuf 43:1311–1317. doi:10.1016/S0890-6955(03)00160-3
29. Grzesik W (1999) Experimental investigation of the influence of adhesion on the frictional conditions in the cutting process. Tribol Int 32:15–23. doi:10.1016/S0301-679X(99)00004-3
30. Singhal V, Litke P, Black A, Garimella S (2005) An experimentally validated thermo-mechanical model for the prediction of thermal contact conductance. Int J Heat Mass Transf 48:5446–5459. doi:10.1016/j.ijheatmasstransfer.2005.06.028